Infrared photodissociation spectroscopy of protonated neurotransmitters in the gas phase

J.P. Simons

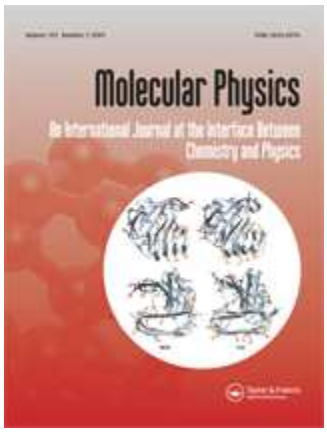

Infrared photodissociation spectroscopy of protonated neurotransmitters in the gas phase

Journal:	*Molecular Physics*
Manuscript ID:	TMPH-2006-0051.R1
Manuscript Type:	Full Paper
Date Submitted by the Author:	26-Oct-2006
Complete List of Authors:	Simons, J.P.; Oxford University, PTCL
Keywords:	spectroscopy

Infrared photodissociation spectroscopy of protonated neurotransmitters in the gas phase.

N. A. MACLEOD[a] and J. P. SIMONS*

Department of Chemistry, Physical and Theoretical Chemistry Laboratory, University of Oxford, South Parks Road, Oxford OX1 3QZ, United Kingdom.

For Molecular Physics Special Issue in Honour of John Brown

*Corresponding author.

E-mail: john.simons@chem.ox.ac.uk

Fax: 01865 275410

[a]Present address.

Central Laser Facility, CCLRC Rutherford-Appleton Laboratories,

Didcot, Oxfordshire OX11 0QZ, UK

Key Words. Protonated ions, spectroscopy, neurotransmitters

7 figures

4 tables.

Abstract.

Protonated neurotransmitters have been produced in the gas phase *via* a novel photochemical scheme: complexes of the species of interest, 1-phenylethylamine, 2-amino-1-phenylethanol and the diastereo-isomers, ephedrine and pseudoephedrine, with a suitable proton donor, phenol (or indole), are produced in a supersonic expansion and ionised by resonant two photon ionisation of the donor. Efficient proton transfer generates the protonated neurotransmitters, complexed to a phenoxy radical. Absorption of infrared radiation, and subsequent evaporation of the phenoxy tag, coupled with time of flight mass spectrometry, provides vibrational spectra of the protonated (and also hydrated) complexes for comparison with the results of quantum chemical computation. Comparison with the conformational structures of the neutral neurotransmitters (established previously) reveals the effect of protonation on their structure. The photochemical proton transfer strategy allows spectra to be recorded from individual laser shots and their quality compares favourably with that obtained using electro-spray or matrix assisted laser desorption ion sources.

1. Introduction

The conformational preferences of neutral ethanolamines and their hydrated complexes, isolated in the gas phase, including 2-amino-1-phenylethanol [1,2], the diastereoisomers ephedrine and pseudoephedrine [3,4], and the catecholamines noradrenaline and adrenaline [5,6] (see Scheme 1), have been characterised recently using a combination of quantum chemical computation, infrared ion-dip spectroscopy and ultraviolet rotational band contour analysis [7]. In every case their favoured structures are stabilised through intramolecular hydrogen bonding (OH $\rightarrow$ N) between the functional groups on the flexible ethanolamine side-chain which preferentially adopts an extended configuration relative to the aromatic ring.

Under physiological conditions the ethanolamine neurotransmitters exist predominantly as protonated ions and their conformational landscapes are radically altered [8-13] but until very recently virtually all direct spectroscopically based structural investigations of biomolecules conducted in the gas phase have focused on neutral molecules and their hydrated complexes [14]. Protonated biomolecular ions, cationic complexes and hydrated ionic complexes simply could not be probed in this way. This has been due, principally, to the problem of generating selectively protonated, and solvated biomolecular ions in sufficient number densities and at low enough temperatures in the gas phase to allow their resolved spectroscopic interrogation and analysis, though their 'averaged shapes' could be explored indirectly, through mass spectrometric ion mobility studies [15,16].

Several ways of overcoming the number density restriction have now been developed, each based upon the coupling of ionisation techniques such as electro-spray

(ESI), or matrix assisted laser desorption (MALDI), [17-25], or electron impact, [26-33] or electrical discharge [34-38] with mass filtering, and cumulative storage in ion traps to enhance their number densities. Their molecular structures have been probed through resonant single, or multiphoton infrared photodissociation spectroscopy. In general, single photon absorption is sufficient for dissociation of weakly bound complexes (typically, with 'reporter' partners such as Ar, N_2 or H_2O) [26-38] but resonantly enhanced multi-photon absorption is required to fragment the bare, uncomplexed ions or proton bound complexes [17, 21, 22]. Comparisons with high-level quantum chemical calculations facilitate spectral assignments to specific structures and the sensitivity of their near infrared bands, in particular those associated with OH and NH stretching modes, to local hydrogen bonded environments, identifies specific inter- and intra-molecular interactions.

An alternative and experimentally simpler, photochemical strategy for the creation of singly protonated ions avoids the need for mass filters and ion traps [39, 40] and follows the sequence shown in Scheme 2. This photochemical strategy is based upon efficient, exothermic proton transfer within an ionised donor-acceptor complex $[AH…B]^+$ to produce the protonated species, BH^+, tagged through hydrogen bonding to the radical, $[BH^+…A]$, step 2 in Scheme 2. Absorption of infra-red radiation, monitored by loss of the radical "tag", step 3, provides an infra-red fingerprint of the 'tagged' protonated species. The strategy is a close relative of the method developed by Dopfer [38], involving proton transfer from Lewis acids such as H_3^+ to weakly bound or hydrogen bonded molecular complexes, recently used for example, to generate the near IR spectra of protonated imidazole tagged with one or two hydrogen bonded water

molecules, [Imid.H^+.$(H_2O)_{1,2}$]. The future inclusion of step 4 in Scheme 2, 'vibrationally assisted' photodissociation [41] using, for example, tunable IR +1064 nm or 532 nm radiation, will offer a means of generating IR spectra of *bare* protonated species.

In the initial "proof of principle" stage of development, using steps 1 – 3 only, the new strategy has enabled the generation, IR spectroscopic detection and in combination with quantum chemical computations, structural assignment of 'phenoxy tagged' protonated 2-aminoethanol [40]; the phenoxy 'reporter' was found to exert only a minimal effect on the geometry of the protonated species to which it was attached, despite the strong hydrogen bond linking it to the protonated ion. The present paper develops this initial study firstly, to enhance the sensitivity of the technique; then to apply it to a series of (tagged) protonated neurotransmitters, including 2-amino-1-phenylethanol (a noradrenaline analogue), ephedrine and its mono-hydrate, and pseudoephedrine, as well as protonated 1-phenylethylamine and imidazole (see Scheme 1).

2. Methodology

The experimental techniques employed follow those used previously [40]. Mixtures of the proton donor (phenol) and proton acceptor were heated (80-100 °C) and expanded in dry (or moistened) helium or argon through a pulsed molecular valve (General Valve, orifice diameter 0.5 mm). The resulting supersonic beam was skimmed (Beam Dynamics, diameter 1 mm) and intersected by two laser beams in the ion-source region of a linear time-of-flight mass spectrometer (R.M. Jordan). Tuneable UV radiation (270-280 nm) was produced by the frequency doubled output of a YAG pumped dye laser (Spectra-Physics GCR-170 and LAS-105) while IR radiation (2.5-3.5 μm) was produced by difference frequency mixing (in a lithium niobate crystal) of the output of a

YAG pumped dye laser (Continuum Powerlite 8010, ND6000 and IRP module) with the YAG fundamental. Typical pulse energies were ~0.5 mJ (UV) and ~4 mJ (IR).

Time-of-flight mass spectra of the complex, phenol…imidazole$^+$, [P-Imid]$^+$, recorded in the presence and absence of IR radiation are shown for illustration in Figure 1, together with its infrared photodissociation spectrum. Although ion peaks associated with the binary complex [P-Imid]$^+$ and bare protonated imidazole, Imid-H$^+$, generated through spontaneous dissociation, were both observed in the absence of IR radiation fragmentation of the complex was enhanced by infrared absorption at 3483 cm^{-1}, (corresponding to one of the NH bands in the IR spectrum of the ionic complex).*

Substantial gains in the signal to noise ratio were obtained by delaying the IR pulse by 300-400 ns relative to the UV laser pulse. During this time the ion population was accelerated towards the detector; absorption of infrared radiation, and subsequent dissociation of the complex, produced the fragment ion, Imid-H$^+$ at a different position of the extraction region, resulting in an arrival time distinct from that of ions produced by spontaneous dissociation following UV excitation alone, see Figure 1. This 'offset' allowed the IR photo-fragment channel and hence the IR absorption spectrum of the parent ion, to be recorded against a near zero background, providing a substantial improvement in the signal to noise. Thus the weak cluster of features centred around 3160 cm^{-1}, associated with the overlapping CH stretching modes of protonated imidazole [33] were clearly observed in the fragment channel, spectrum (a), but were submerged in the background noise of the spectrum measured by depletion of the parent ion, spectrum (b). This experimental "trick" allowed high-quality spectra of protonated species to be

* The ion peaks associated with phenol (P$^+$), its mono-hydrate (P.H$_2$O)$^+$ and its dimer (P$_2$)$^+$, which also appeared in the time of flight spectrum, conveniently facilitated accurate mass calibration

recorded quickly and efficiently without the need for a more complex experimental system of mass filters or ion traps.

Quantum chemical computations were performed using the GAUSSIAN 03 program [41]. Initial structures of bare protonated amines and their complexes with the phenoxy radical were optimised using density functional theory (B3LYP functional with a 6-31+G* basis set) and their harmonic vibrational wavenumbers were computed. Single point MP2/6-311++G** calculations, which included a (harmonic) zero point energy correction, provided their relative energies. Infrared frequencies associated with the OH and NH stretch modes were scaled by 0.976 and 0.956, respectively, following previous practice [1 – 6].

The conformational notation, A/G refers to the arrangement (*Anti* or *Gauche*) of the $C_{arom}C_{\alpha}C_{\beta}N$ and $OC_{\alpha}C_{\beta}N$ atom chains, respectively (see Scheme 1). The labels 'a' and 'b' reflect the inversion of the (chiral) methyl-amino group in ephedrine and pseudoephedrine, which results in a doubling of the conformational space. Complexes with the phenoxy radical are denoted by the mode of clustering: addition to a non-hydrogen bonded NH group (NH-add), or insertion across the intramolecular hydrogen bonds between NH and O of the side-chain (NH-ins), or between the NH and the π-system of the aromatic ring (π-ins).

3. Results

3.1. Overview

The initial geometry optimisations (B3LYP/6-31+G*) of the cationic complexes of the three neurotransmitters and of 1-phenylethylamine, starting from the optimised neutral geometries of hydrogen bonded, AH → N structures, resulted in facile proton

transfer, leading to structures of the type [A…H^+B]. Alternative starting geometries in which the phenol was hydrogen bonded to the hydroxyl group, AH → O, in the ethanolamine acceptors led to the cationic or charge-transferred structures, [AH^+…B] or [AH…B^+]. In common with complexes involving the generic acceptor, 2-aminoethanol [39, 40] these structures were located at substantially higher relative energies, ~50-100 kJ mol^{-1}, and their computed vibrational spectra did not reproduce the experimental data.

Near infrared photodissociation spectra of the series of cationic complexes, recorded in each case *via* the delayed fragment channel, are collected together in Figure 2; those generated by the ethanolamines are similar to the spectrum obtained previously for 2-aminoethanol, as expected for a proton transferred structure. They all display a band centred at ~3650 cm^{-1}, associated with a non-hydrogen bonded 'free' alcoholic OH group (*c.f.* ethanol) and two bands (in 2-amino-1-phenylethanol) or a single band (in the ephedra) associated with non-hydrogen bonded or *intra*-molecular hydrogen-bonded (NH^+ → OH) amino groups, appearing in the region 3200-3300 cm^{-1}. The onset of the broad and intense band associated with the intermolecular hydrogen bond, NH^+ → OPh, linking the protonated ion to the phenoxy radical, anticipated at low wavenumbers, <3000 cm^{-1}, is clearly evident in the spectrum associated with 1-phenylethylamine. The inset in Figure 2 compares the IR features associated with the OH band, generated through photodissociation of two alternative proton donor complexes, [ephedrine-phenol]$^+$ and [ephedrine-indole]$^+$. The two spectra are virtually identical, reinforcing the view that the 'tag', be it the phenoxy or the de-protonated indole residue, does not significantly perturb its protonated partner.

The widths of the OH and NH band contours, 20-40 cm^{-1} FWHM, are substantially greater than those recorded in ion-dip experiments of the corresponding jet-cooled neutral species, ~5 cm^{-1} [1-7]. The broader widths are a consequence of the production method. Resonant one-colour two-photon ionisation promotes an exothermic proton transfer step (typically ~60 kJ mol^{-1} for a primary or secondary amine) [43, 44] to create a spread of internal energies in the protonated ion complex [A…H^+B] which extends beyond its dissociation threshold – hence the spontaneous generation of the bare protonated BH^+ ions detected in the t.o.f. mass spectra: the infra-red photodissociation spectra reflect the excitation of a succession of unresolved 'hot' sequence bands.

3.2. 1-Phenylethylamine (PEA)

Computed (B3LYP/6-31+G*) structures of bare PEA.H^+ and its phenoxy complex are shown in Figure 3 and their relative energies and geometrical parameters are given in Table 1. The bare protonated ion displays a single structure with two hydrogen bonds linking the NH_3^+ group to the π-system of the aromatic ring [45] but the complex presents three distinct structures, labelled (a), (b) and (c), all lying within ~4 $kJmol^{-1}$ of the global minimum structure, (a). In each case, the phenoxy 'tag' causes only a mild perturbation to the geometry of the protonated species, see Table 1.

The experimental infra-red photodissociation (IRPD) spectrum of the cationic complex(es), shown in Figure 3, displays two relatively sharp features at 3350 cm^{-1} and 3290 cm^{-1}, and a very broad, red-shifted feature at < 3200 cm^{-1}. They are assigned to the three NH stretching modes expected for a proton transferred structure although it is not possible to estimate their relative contributions, given the good agreement between experiment and computation for each of the three possible complex structures .

3.3. 2-Amino 1-phenyl ethanol (APE)

The lowest-lying computed structures and IR spectra of bare and complexed APE.H^+ are shown in Figure 4, and their relative energies and structural parameters are given in Table 2. There are four potential binding sites in the protonated complex, [PhO…APE.H^+], located at the NH_3^+ and OH groups but in common with protonated 2-aminoethanol [39, 40], structures involving the hydroxyl group are far less energetically favoured (by ~20 kJ mol^{-1}).

In each case the protonated ethanolamine side chain adopts a folded, GG structure in the minimum energy configuration. In the bare ion, APE.H^+, this structure is calculated to lie at an energy ~6 kJ mol^{-1} below that of the extended, AG conformer, in contrast to the neutral molecule, where the AG conformer is marginally favoured [1, 2, 46]. In the 'tagged' ion the minimum energy conformer is associated with two, almost isoenergetic, GG conformational structures, GG-NH-add and GG-π-ins. They are stabilised by an intramolecular, $NH^+ \rightarrow$ OH, hydrogen bond, reversing the principal interaction of the neutral species, and the GG conformation is further stabilised by an $NH^+ \rightarrow \pi$ interaction with the aromatic ring.

The experimental IRPD spectrum of the ionised phenol-APE complex, also shown in Figure 4, displays a band at 3650 cm^{-1} (OH) and two further bands at 3360 cm^{-1} and 3250 cm^{-1} (NH), as expected for the protonated complex, PhO…APE.H^+. The non-bonded OH group is insensitive to conformational change but the spacing of the computed symmetric and antisymmetric NH_2 modes for the two lowest-lying GG complexes are slightly different. The bands at 3360 cm^{-1} and 3250 cm^{-1} are quite broad

and a shoulder on the low frequency side of the peak centred at 3360 cm^{-1} band suggests the population of both structures.

3.4. Ephedrine and Pseudoephedrine

Figures 5 and 6 present the energetically low-lying computed structures of the bare and phenoxy complexed protonated diastereoisomers, ephedrine and pseudoephedrine, together with their near infrared photodissociation spectra. Their relative energies and selected structural data are presented in Tables 3 and 4. Like APE, the protonated conformers are all stabilised by an intramolecular hydrogen bond, $NH^+ \rightarrow$ OH; the folded (GGa) structures also benefit from an interaction with the aromatic ring, $NH^+ \rightarrow \pi$. In protonated ephedrine this strongly favours the folded global minimum conformation, GGa; the extended, AGa conformer, lies ~10 kJ mol^{-1} higher in energy. In contrast, the corresponding structures in the protonated diastereoisomer, *pseudo*ephedrine, are nearly isoenergetic.

Addition of a bound phenoxy radical does not alter their conformational landscapes significantly. The preference for a folded configuration is retained in the protonated ephedrine complex. The global minimum structure, GGa-π-ins, is now also favoured by a π-π interaction between the aromatic rings; the alternative folded structure, GGa-NH-ins, lies ~4 kJmol^{-1} higher in energy. Complexes with extended, AGa side-chain conformations all lie at much higher relative energies (>11 kJ mol^{-1}) again in marked contrast to pseudoephedrine, where the extended (AGb-NH-add) and folded (GGa-π-ins and GGa-NH-ins) complexes all lie within 4 kJ mol^{-1} of the global minimum structure, AGa-NH-add, see Figure 5 and Table 3.

The experimental IRPD spectra shown in Figures 5 and 6 are in substantial agreement with the spectra computed for each of the energetically low-lying phenoxy tagged protonated structures. Given their computed relative energies, the experimental spectrum associated with protonated ephedrine can be assigned predominantly, to the single (folded) structure, GGa-π-ins. The corresponding data for the protonated pseudoephedrine complex(es) do not allow unequivocal structural assignment(s).

3.5 Hydrated ephedrine

Figure 7 presents a 'proof of principle' IR photodissociation spectrum recorded in the 'OH stretch' region, of the hydrated cationic complex of indole and ephedrine, monitored via the depletion of the singly hydrated ion peak, [indole..ephedrine..H_2O]$^+$ and also via the enhancement of the fragment ion, [indole..ephedrine]$^+$. The computed global minimum structure of the untagged hydrated ion, [ephedrine.H^+…H_2O], is also shown. Like the free ion, ephedrine.H^+, the folded GGa conformation is strongly favoured; the relative energy calculated for the lowest-lying extended conformation, AGb, is ~5 kJ mol^{-1}. In both cases the DFT calculations generate a structure in which the water molecule is bound via a linear H-bond to the protonated amino group: the protonated ion is predicted to display symmetric and antisymmetric OH bands at ~3625 cm^{-1} and ~3750 cm^{-1}, respectively, while the OH group on the protonated ephedrine remains at ~3645 cm^{-1}. The experimental IR photodissociation spectrum of the tagged ion suggests a more complex structure. The (unshifted) band at ~3650 cm^{-1} corresponds well with an assignment to the OH group on the ethanolamine side chain, but the location of the other two bands, between ~3,700 cm^{-1} and 3,750 cm^{-1}, suggests a perturbed

structure, most likely involving an interaction between the bound water molecule and the lone pair electrons on the hydroxyl group of the ephedrine or the indole residue.

4. Discussion

4.1. Conformational landscapes

The conformational landscapes of the protonated molecules are the product of a subtle balance between a number of competing, and cooperative effects including intramolecular hydrogen bonding, predominantly $NH^+ \rightarrow O$ and $NH^+ \rightarrow \pi$, but also other non-bonded interactions including butane-like interactions between neighbouring methyl groups and between the *N*-methyl group and the aromatic ring in ephedrine and pseudoephedrine. These types of interaction also shape the conformational landscape of the neutral species [1-7] but the outcome can be radically altered by protonation. The diastereoisomers, ephedrine and pseudoephedrine provide a good case study.

In the neutral ethanolamines [3] and in protonated pseudoephedrine, the energies of the two lowest-lying folded and extended conformers, GGa and AGa, are very similar. Protonation of ephedrine, however, increases their relative energies (from 3 kJ mol^{-1} to 11 kJ mol^{-1}) and switches the favoured conformation from an extended, AGa, to a folded, GGa, configuration. A similar trend is found for neutral [1,2] and protonated APE. The most apparent change in bonding following protonation is a reversal in the direction of the intramolecular hydrogen bond of the ethanolamine side-chain from $OH \rightarrow N$ in the neutral to $NH^+ \rightarrow OH$ in the protonated ion. This is reflected in the displacement of the corresponding vibrational transitions: in the neutral ethanolamines, ν(OH) shifts towards low wavenumbers, located at ~3520 cm^{-1} and the ν(NH) band appears at ≈3430 cm^{-1} but in the protonated ions ν(OH) is found at ≈3650 cm^{-1} but the ν(NH) band(s) shift towards

lower wavenumbers, typically ~3250-3350 cm^{-1}. Their folded geometries also benefit from an interaction between the protonated amino group and the aromatic ring, $NH^{+} \rightarrow \pi$.

The preference for a folded configuration in protonated ephedrine, and APE.H^{+} indicated by computation with some support from experiment, is perhaps unsurprising when the energetics of the competing interactions are estimated. The interaction energy of the ammonium ion, NH_4^{+} with water (~75 kJ mol^{-1}) [47-50] or with benzene (~70 kJ mol^{-1}) [51,52] is an order of magnitude greater than that of the butane-like methyl-methyl interaction (~5 kJ mol^{-1}) [53-55] and substantially greater than that associated with hydrogen bonded interactions in neutral molecules (*e.g.* ~25 kJ mol^{-1} for HOH $\rightarrow$ NH_3 and ~8 kJ mol^{-1} for NH_3 $\rightarrow$ benzene [56,57]). While the hydrogen bonds in the protonated ephedrines are far from optimal because of the geometrical constraints, NH^{+}…O distances and angles ~200 pm and ~110°, *cf.* 160 pm and 180° in $NH_4^{+} \rightarrow OH_2$ [57], the additional interaction with the aromatic ring in the folded GGa conformation readily compensates the unfavourable *gauche* arrangement of the neighbouring methyl groups. This contrasts with the neutral ephedrines, where the stabilisation provided by an NH $\rightarrow$ π hydrogen bond with the aromatic ring is much smaller and is of a similar magnitude to the energy difference between the *trans* and *gauche* configurations of the neighbouring methyl groups [3]. The change in absolute configuration of one of the chiral carbon centres, from (1R,2S)-ephedrine to (1S,2S)-pseudoephedrine, and the subsequent modulation of the non-covalent interaction between the methyl groups, has a significant effect on the relative stabilities of the folded and extended configurations.

The behaviour of protonated pseudoephedrine, where the folded and extended conformers are almost isoenergetic, can be rationalised by the influence of competing

interactions in the folded, GGa, structure. Optimisation of the geometry for one intramolecular hydrogen bond can only be achieved by sacrificing, at least to some degree, the other. The $NH^+ \rightarrow O$ hydrogen bond is markedly longer in the GGa conformer of protonated pseudoephedrine than in the other structures: 220 pm and 103° *versus* ~200 pm and ~110°. Conversely the interaction with the aromatic ring is stronger: the NH^+…'centre of ring' distance and angle is ~320 pm and 130° (*c.f.* ~350 pm and 120° for the GGa conformer of protonated ephedrine) although still far from optimal (*c.f.* ~220 pm and ~160° in $NH_4^+ \rightarrow$ benzene [57]). The deciding factor is the interaction between the neighbouring methyl groups which is controlled by the absolute chirality of the molecule. In pseudoephedrine, "optimisation" of the geometry of the $NH^+ \rightarrow O$ hydrogen bond would require the methyl groups to adopt a more eclipsed form while the opposite is true for the $NH^+ \rightarrow \pi$ hydrogen bond. Switching of the configuration about a single chiral carbon, in ephedrine, reverses this dependence. The result, in the GGa conformer of pseudoephedrine, is two geometrically non-optimal hydrogen bonds and the raising of the energy of the folded structure relative to that of the extended AGa conformer.

4.2. Comments on future applications of the photochemical protonation method

Using the phenol (or indole) cation as a proton source within a molecular complex provides a means of producing spectroscopically useful number densities of 'tagged' protonated biomolecules in the gas-phase. Combination of the photochemical proton transfer mechanism, time of flight mass spectrometry and IRPD detection allows data to be recorded in single laser shots without the need for ion trapping; the spectra presented in the present article were collected in a matter of hours without compromising signal to noise. It is now possible to record infrared fingerprints of a wide range of protonated

biomolecular ions in the gas phase (including for example, both aliphatic and aromatic amino acids and small peptides, using laser ablation sources [58]) with a relatively simple experimental arrangement. The future implementation of the 'vibrationally assisted' photo-dissociation step (4) promises spectroscopic access to the bare ions as well.

On the negative side (but see below) the resolution is currently inferior to that provided by infrared ion-dip spectroscopy of jet-cooled neutral molecules [1-7, 14] and protonated molecular complexes [26-38] and the width of the spectral bands limits the ability to distinguish between species with similar vibrational spectra. The NH stretch region of APE where a partially resolved shoulder on the principal band (3360 cm^{-1}) was tentatively assigned to an alternative complex, see Figure 4, provides a good example. The combination of excess energy from the 2-photon excitation process, ~100 kJ mol^{-1}, depending on the ionisation energy of the complex and the kinetic energy of the ejected photoelectron [39, 40], with the energy released from the proton transfer reaction, ~50 kJ mol^{-1}, [43, 44] results in substantial internal excitation of the complex. Single-point MP2/6-311++G** energy calculations on the DFT optimised geometries indicate binding energies ~100 kJ mol^{-1}, well within the estimated upper limit of the internal energy, ~150 kJ mol^{-1}. Given the levels of internal excitation the relative populations of contributing conformations may be dictated both by entropic and enthalpic factors.

Fortunately, a number of experimental improvements are in prospect, promising amelioration of some of these constraints, particularly the production of internally cooled, untagged protonated ions, which requires ionisation of the proton donor within the collision region of a supersonic expansion and their selective detection by resonant, vibrationally assisted photodissociation. The potential for future development, coupled

with the simplicity and efficiency of the experiment, promise to make the photochemical scheme an attractive companion to more established methods for the spectroscopic examination of many protonated biomolecules, particularly in the small molecule region (< 1000 amu).

5. Conclusions

A new photochemical method has been used to record the near IR spectra of a series of protonated neurotransmitters, including the noradrenaline analogue, 2-amino-1-phenylethanol, the diastereoisomers ephedrine and pseudoephedrine, and 1-phenylethylamine, in the gas-phase. Photoionisation of the phenol chromophore in a molecular complex and subsequent proton transfer to the amine partner provides an efficient and selective means of producing protonated ions which avoids the need for mass filters and ion traps. Spectroscopic information has been obtained using infrared photodissociation of the complex between the protonated species and the phenoxy fragment to provide a near IR spectrum of the protonated molecule. The spectra are comparable in quality and bandwidth with those obtained using ESI or MALDI sources while the efficiency of the proton transfer and the ability to obtain high-quality spectroscopic data quickly, provide a significant gain in sensitivity and saving in time

DFT and *ab initio* quantum chemical computations allow the assignment of experimental spectra to specific conformers or groups of conformers which in turn, allow detailed analysis of their conformational landscapes. Comparisons with the preferred conformations of neutral ethanolamines have revealed the influence of protonation on their conformational structures. The preferred side-chain structure in ephedrine is altered by protonation, from an extended to a folded configuration but in its diastereoisomer,

pseudoephedrine (differing only in the chirality of a single carbon), their relative potential energies remain closely spaced. The preferred side chain conformations are controlled by a delicate balance between different non-bonded interactions, including intramolecular $NH^+ \rightarrow O$ and $NH^+ \rightarrow \pi$ hydrogen bonding and methyl-methyl interactions; the conformational landscapes are also sensitive to, and can be altered by the local configuration about chiral centres.

Acknowledgements

This article is dedicated to Professor John Brown. It has been a great privilege to work in the same Department, share the same laboratory and College, and benefit from his knowledge, enthusiasm, encouragement, and kindness. We thank Dr Romano Kroemer for providing us with the computed data for the complex between protonated ephedrine and water, Drs Timothy Vaden and Lavina Snoek for helpful discussions, the Leverhulme Trust for financial support (grant F/8788G), the Lasers for Science facility of the CCLRC for the loan of a UV laser system, and the support provided by the Physical and Theoretical Chemistry Laboratory in Oxford.

References.

[1] R. J. Graham, R. T. Kroemer, M. Mons, E. G. Robertson, L. C. Snoek and J. P. Simons, J. Phys. Chem. A., **103**, 9706 (1999).

[2] N. A. Macleod, E. G. Robertson and J. P. Simons Mol. Phys., **101**, 2199 (2003).

[3] P. Butz, R. T. Kroemer, N. A. Macleod and J. P. Simons, J. Phys. Chem. A., **105**, 544 (2001).

[4] P. Butz, R. T. Kroemer, N. A. Macleod and J. P. Simons, Phys. Chem. Chem. Phys., **4**, 3566 (2002).

[5] L. C. Snoek, T. van Mourik and J. P. Simons, Mol. Phys., **101**, 1239 (2003).

[6] P. Çarçabal, L. C. Snoek and T. van Mourik, Mol. Phys., **103**, 1633 (2005).

[7] E. G. Robertson and J. P. Simons, Phys. Chem. Chem. Phys., **3**, 1 (2001).

[8] J. M. Berg, J. L. Tymoczko and L. Stryer, *"Biochemistry",* 5th edition, W.H. Freeman, New York, (2002).

[9] P. I. Nagy and K. Takacs-Novak, Phys. Chem. Chem. Phys., **6**, 2838 (2004).

[10] P. I. Nagy, G. Alagona, C. Ghio and K. Takacs-Novak, J. Am. Chem. Soc., **125**, 2770 (2003).

[11] M. Ramek and P. I. Nagy, J. Phys. Chem. A., **104**, 6844 (2000).

[12] P. I. Nagy, G. Alagona and C. Ghio, J. Am. Chem. Soc., **121**, 4804 (1999).

[13] J. P. Simons, C. R. Chimie, **6**, 17 (2003).

[14] See for example, *"Bioactive molecules in the gas phase",* Phys. Chem. Chem. Phys., **6**, 2543 (2004).

[15] J. Gidden, P. Kemper, E. Shammel, D. P. Fee, S. Anderson and M. T. Bowers, Int. J. Mass Spectrom., **222**, 63 (2003).

[16] D. E. Clemmer and M. F. Jarrold, J. Mass Spectrom., **32**, 577 (1997).

[17] H .B. Oh, C. Lin, H. Y. Hwang, H. Zhai, K. Breuker, V. Zabrouskov, B.K. Carpenter and F. W. McLafferty, J. Am. Chem. Soc., **127**, 4076 (2005).

[18] B. Lucas, G. Gregoire, J. Lemaire, P. Maitre, F. Glotin, J. P. Schermann and C. Desfrancois, Int. J. Mass. Spectrom., **243**, 105 (2005).

[19] B. Lucas, G. Gregoire, J. Lemaire, P. Maitre, J. M. Ortega, A. Rupenyan, B. Reimann, J. P. Schermann and C. Desfrancois, Phys. Chem. Chem. Phys., **6**, 2659 (2004).

[20] N. C. Polfer, B. Paizs, L. C. Snoek, I. Compagnon, S. Suhai, G. Meijer, G. von Helden and J. Oomens, J. Am. Chem. Soc., **127**, 8571 (2005).

[21] J. Oomens, N. Polfer, D. T. Moore, L. van der Meer, A. G. Marshall, J. R. Eyler, G. Meijer and G. von Helden, Phys. Chem. Chem. Phys., **7**, 1345 (2005).

[22] L. MacAleese, A. Simon, T. B. McMahon, J. M. Ortega, D. Scuderi, J. Lemaire and P. Maitre, Intl. J. Mass Spectrometry, **249**, 14 (2006).

[23] C. Marian, D. Nolting and R. Weinkauf, Phys. Chem. Chem. Phys., **7**, 3306 (2005).

[24] D. Nolting, C. Marian and R. Wienkauf, R., Phys. Chem. Chem. Phys., **6**, 2633 (2004).

[25] F. O. Talbot, T. Tabarin, R. Antoine, M. Broyer and P. Dugourd, J. Chem. Phys., **122**, 074310 (2005).

[26] N. Solcà and O. Dopfer, J. Phys. Chem. A., **109**, 6174 (2005).

[27] N. Solcà and O. Dopfer, J. Chem. Phys., **121**, 769 (2004).

[28] N. Solcà and O. Dopfer, J. Chem. Phys., **120**, 10470 (2004).

[29] N. Solcà and O. Dopfer, J. Am. Chem. Soc., **126**, 1716 (2004).

[30] N. Solcà and O. Dopfer, Chem. Eur. J., **9**, 3154 (2003).

[31] N. Solcà and O. Dopfer, Angew. Chem. Int. Ed., **42**, 1537 (2003).

[32] N. Solcà and O. Dopfer, J. Am. Chem. Soc.,**125**, 1421 (2003).

[33] H. S.Andrei, N. Solcà and O. Dopfer, ChemPhysChem, **7**, 107 (2006).

[34] C.C. Wu, C. Chaudhuri, J.C. Jiang, Y.T. Lee and H.C. Chang, J. Phys. Chem. A., **108**, 2859 (2004).

[35] C. C. Wu, C. Chaudhuri, J. C. Jiang, Y. T. Lee and H. C. Chang, Mol. Phys., **101**, 1285 (2003).

[36] K. Y. Kim, H. C. Chang, Y. T. Lee, V. I. Cho and D. W. Boo, J. Phys. Chem. A., **107**, 5007 (2003).

[37] C. C. Wu, J. C. Jiang, I. Hahndorf, C. Chaudhuri, Y. T. Lee and H. C. Chang, J. Phys. Chem. A., **104**, 9556 (2000).

[38] C. C. Wu, J. C. Chiang, D. W. Boo, S. H. Lee, Y. T. Lee and H. C. Chang, J. Chem. Phys., **112**, 176 (2000).

[39] N. A. Macleod and J. P. Simons, Phys. Chem. Chem. Phys., **5**, 1123 (2003).

[40] N. A. Macleod and J. P. Simons, Phys. Chem. Chem. Phys., **6**, 2821 (2004).

[41] F. F. Crim, F. F., Ann. Rev. Phys. Chem., **44**, 397 (1993).

[42] Gaussian 03, Revision C.02, M. J. Frisch, G. W. Trucks, H. B. Schlegel, G. E. Scuseria, M. A. Robb, J. R. Cheeseman, J. A. Montgomery, Jr., T. Vreven, K. N. Kudin, J. C. Burant, J. M. Millam, S. S. Iyengar, J. Tomasi, V. Barone, B. Mennucci, M. Cossi, G. Scalmani, N. Rega, G. A. Petersson, H. Nakatsuji, M. Hada, M. Ehara, K. Toyota, R. Fukuda, J. Hasegawa, M. Ishida, T. Nakajima, Y. Honda, O. Kitao, H. Nakai, M. Klene, X. Li, J. E. Knox, H. P. Hratchian, J. B. Cross, C. Adamo, J. Jaramillo, R. Gomperts, R. E. Stratmann, O. Yazyev, A. J. Austin, R. Cammi, C. Pomelli, J. W. Ochterski, P. Y. Ayala, K. Morokuma, G. A. Voth, P. Salvador, J. J. Dannenberg, V. G. Zakrzewski, S. Dapprich, A. D. Daniels, M. C. Strain, O. Farkas, D. K. Malick, A. D. Rabuck, K. Raghavachari, J. B. Foresman, J.

V. Ortiz, Q. Cui, A. G. Baboul, S. Clifford, J. Cioslowski, B. B. Stefanov, G. Liu, A. Liashenko, P. Piskorz, I. Komaromi, R. L. Martin, D. J. Fox, T. Keith, M. A. Al-Laham, C. Y. Peng, A. Nanayakkara, M. Challacombe, P. M. W. Gill, B. Johnson, W. Chen, M. W. Wong, C. Gonzalez, and J. A. Pople, Gaussian, Inc., Wallingford CT, (2004).

[43] E.P. Hunter and S.G. Lias, "Proton Affinity Evaluation" in NIST Chemistry WebBook, NIST Standard Reference Database Number 69, Eds. P.J. Linstrom and W.G. Mallard, June 2005, National Institute of Standards and Technology, Gaithersburg MD, 20899 (http://webbook.nist.gov).

[44] H. T. Kim, R. J. Green, J. Qian and S. L. Anderson, J. Chem. Phys., **112**, 5717 (2000).

[45] N. A. Macleod, P. Butz, J. P. Simons, G. H. Grant, C. M. Baker and G. E. Tranter, Phys. Chem. Chem. Phys., **7**, 1432 (2005).

[46] T. F. Miller and D. C. Clary, J. Phys. Chem. B., **108**, 2484 (2004).

[47] F. C. Pickard, M. E. Dunn and G. C. Shields, J. Phys. Chem. A., **109**, 4905 (2005).

[48] H. M. Lee, P. Tarakeshwar, J. Park, M. R. Kolaski, Y. J. Yoon, H. B. Yi, W. Y. Kim and K. S. Kim, J. Phys. Chem. A., **108**, 2949 (2004).

[49] J. C. Jiang, H. C. Chang, Y. T. Lee and S. H. Lin, J. Phys. Chem. A., **103**, 3123 (1999).

[50] F. Bruge, M. Bernasconi and M. Parrinello, J. Chem. Phys., **110**, 4734 (1999).

[51] M. Aschi, F. Mazza and A. Di Nola, J. Mol. Struct (THEOCHEM), **587**, 177 (2002).

[52] C. A. Deakyne and M. Meot-Ner, J. Am. Chem. Soc., **107**, 474 (1985).

[53] J. R. Durig, C. Aheng, W. A. Herrebout and B. J. van der Veken, J. Mol. Struct., **641**, 207 (2002).

[54] J. K. Badenhoop and F. Weinhold, Int. J. Quantum Chem., **72**, 269 (1999).

[55] N. L. Allinger, J. T. Fermann, W. D. Allen and H. F. Schaefer, J. Chem. Phys., **106**, 5143 (1997).

[56] S. Tsuzuki and H. P. Luthi, J. Chem. Phys., **114**, 3949 (2001).

[57] M. Mons, I. Dimicoli, B. Tardivel, F. Piuzzi, V. Brenner and P. Millié, Phys. Chem. Chem. Phys., **4**, 571 (2002).

[58] N. A. Macleod, E. M. Marzluff, and J. P. Simons, work in progress.

Table Captions

Table 1. Computed relative energies, dihedral angles and hydrogen bond distances/angles for protonated 1-phenyl ethylamine (PEA) and its complexes with the phenoxy radical: (i) MP2/6-311++G**//B3LYP/6-31+G*, (ii) B3LYP/6-31+G* optimisation.

Table 2. Computed relative energies, dihedral angles and hydrogen bond distances/angles for protonated 2-amino 1-phenylethanol (APE) and its complexes with the phenoxy radical: (i) MP2/6-311++G**//B3LYP/6-31+G*, (ii) B3LYP/6-31+G* optimisation.

Table 3. Computed relative energies, dihedral angles and hydrogen bond distances/angles for protonated ephedrine (Eph) and its complexes with the phenoxy radical: (i) MP2/6-311++G**//B3LYP/6-31+G*, (ii) B3LYP/6-31+G* optimisation.

Table 4. Computed relative energies, dihedral angles and hydrogen bond distances/angles for protonated pseudoephedrine (Peph) and its complexes with the phenoxy radical: (a) MP2/6-311++G**//B3LYP/6-31+G*, (b) B3LYP/6-31+G* optimisation.

	$PEA.H^+$	$PhO…PEA.H^+$		
		add (a)	*add (b)*	*add (c)*
ΔE / kJ mol^{-1} (i)	-	0.0	2.7	3.6
$\angle C_2C_i\text{-}C_\alpha C_\beta$ /^{o} (ii)	-43	-49	-53	-46
PhO…HN /pm (ii)	-	167	170	169
$\angle$ PhO-HN /^{o} (ii)	-	162	174	172

Table 1.

	APE.H$^+$		PhO...APE.H$^+$			
	GG	*AG*	*GG-NH-add*	*GG-π-ins*	*GG-NH-ins*	*AG-NH-add-(a)*
ΔE / kJ mol^{-1} (i)	0.0	6.1	0.0	0.1	2.7	3.6
$C_{arom}C_\alpha C_\beta N$ /^{o} (ii)	69	169	68	73	61	172
$OC_\alpha C_\beta N$ /^{o} (ii)	-54	46	-55	-51	-63	49
NH…O /pm (ii)	219	202	227	212	269	210
∠ NH-O /^{o} (ii)	105	111	104	110	87	110
PhO..HN /pm (ii)	-		167	171	166	168
∠PhO-HN /^{o} (ii)	-		165	152	158	164

Table 2.

	Eph.H^+ *GGa*	PhO...Eph.H^+ *GGa-π-ins*	*GGa-NH-ins*
ΔE / kJ mol^{-1} (i)	0.0	0.0	4.4
$C_{arom}C_\alpha C_\beta N$ /° (ii)	-71	-74	-62
$OC_\alpha C_\beta N$ /° (ii)	53	51	62
$CC_\beta NC$ /° (ii)	67	82	56
NH…O /pm (ii)	204	204	241
∠ NH-O /° (ii)	114	115	101
PhO…HN /pm (ii)	-	178	177
∠PhO-HN /° (ii)	-	153	148

Table 3.

	Peph.H$^+$		PhO...Peph.H$^+$			
	GGa	*AGa*	*AGa-NH-add*	*GGa-π-ins*	*GGa-NH-ins*	*AGb-NH-add*
ΔE / kJ mol^{-1} (i)	0.0	1.1	0.0	1.2	1.4	3.7
$C_{arom}C_\alpha C_\beta N$ /^{o} (ii)	66	167	169	72	61	165
$OC_\alpha C_\beta N$ /^{o} (ii)	-57	44	46	-53	-63	42
$CC_\beta NC$ /^{o} (ii)	62	76	71	45	76	-53
NH…O /pm (ii)	225	192	199	211	268	203
∠ NH…O /^{o} (ii)	103	117	114	111	88	112
PhO…HN /pm (ii)	-		174	179	173	173
∠PhO…HN /^{o} (ii)	-		169	150	156	167

Table 4.

Scheme and Figure Captions.

Scheme 1. Molecular structures of ethanolamines

Scheme 2. Photochemical production and spectroscopic detection of protonated ions in the gas-phase.

1. Complexes of the biomolecule of interest (B) with a proton donor (AH) are produced in a cold molecular beam and ionised by resonant UV two-photon ionisation.
2. Exothermic, proton transfer within the cation generates the protonated biomolecule (H^+B), initially complexed with a radical (A).
3. The complexes fragment, either thermally or through infrared photon excitation. The IR 'photo-dissociation spectrum' provides an absorption spectrum of the weakly bound, protonated biomolecular complex, A…H^+B.
4. The free protonated biomolecule can also be dissociated through resonant, vibrationally mediated excitation (IR + visible or UV) or multiphoton IR excitation to generate a vibrational spectrum of the *free* ion, BH^+.

Comment [P1]: Change "nhv(IR)" on the scheme, to "IR + nhv"

Figure 1. (a) Time-of-flight mass spectra and (b) infra-red photodissociation spectra of the cationic complex between phenol and imidazole.

Figure 2. Infra-red photodissociation spectra of the cationic complexes between phenol and a variety of amines, including 1-phenylethylamine (PEA), 2-amino-1-phenylethanol (APE) and the diastereoisomers ephedrine (Eph) and pseudephedrine (Peph). Inset shows spectra generated by photo-dissociation of $[phenol\text{-}ephedrine]^+$ and $[indole\text{-}ephedrine]^+$ complexes.
The apparent structure on the bands around 3650 cm^{-1} is the result of a reduction in infra-red power by atmospheric water absorption.

Figure 3. Infra-red photodissociation spectrum of the cationic complex between phenol and 1-phenylethylamine and corresponding spectra computed for the low-lying conformers of protonated PEA and its complexes with the phenoxy radical. The intensity of the strongly hydrogen bonded NH group (NH → OPh) at ~2900 cm^{-1}, has been reduced by a factor of 10 for clarity.

Figure 4. Infra-red photodissociation spectrum of the cationic complex between phenol and 2-amino-1-phenylethanol (APE) and corresponding spectra computed for the low-lying conformers of protonated APE and its complexes with the phenoxy radical. The intensity of the strongly hydrogen bonded NH group at ~ 2800 cm^{-1} has been reduced by a factor of 10 for clarity.

Figure 5. Infra-red photodissociation spectrum of the cationic complex between phenol and ephedrine (Eph) and corresponding spectra computed for the low-lying conformers of protonated Eph and its complexes with the phenoxy radical. The intensity of the strongly hydrogen bonded NH group at ~ 3000 cm^{-1} has been reduced by a factor of 10 for clarity.

Figure 6. Infra-red photodissociation spectrum of the cationic complex between phenol and pseudoephedrine (Peph) and corresponding spectra computed for the low-lying conformers of protonated Peph and its complexes with the phenoxy radical. The intensity of the strongly hydrogen bonded NH group at ~ 3000 cm^{-1} has been reduced by a factor of 10 for clarity.

Figure 7. Infra-red photodissociation spectrum of the cationic complex, between indole and singly hydrated ephedrine, [indole…ephedrine…H_2O]$^+$, recorded in the 'OH stretch' region, and computed structure of the free, hydrated ion.

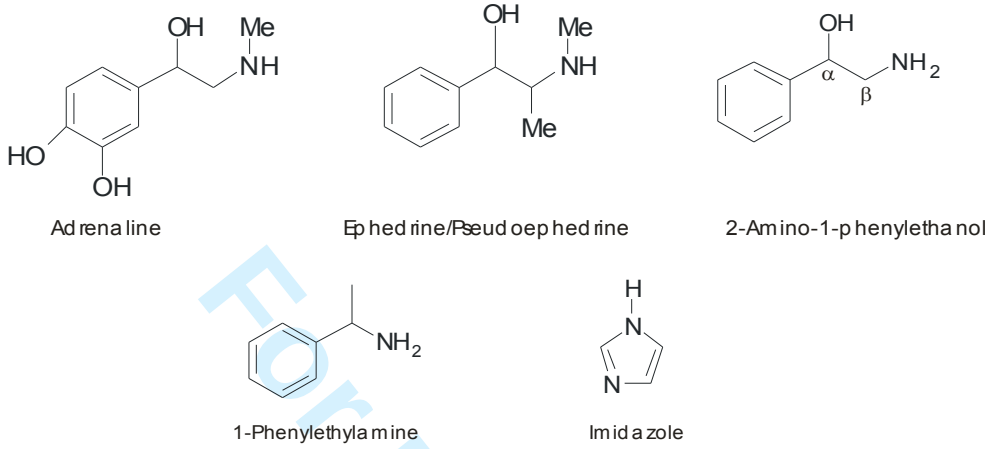

Scheme 1.

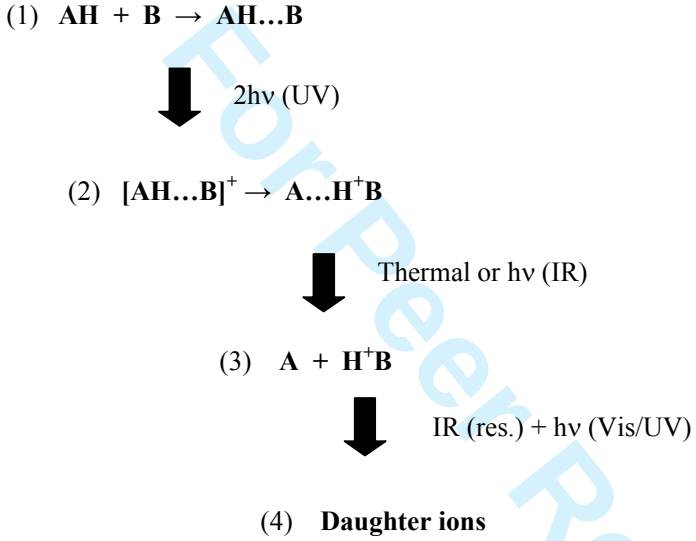

Scheme 2.

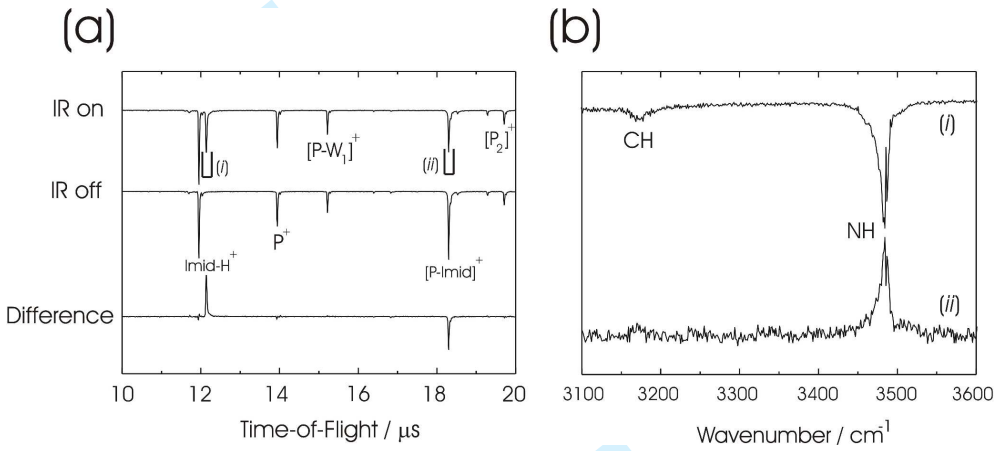

Figure 1.

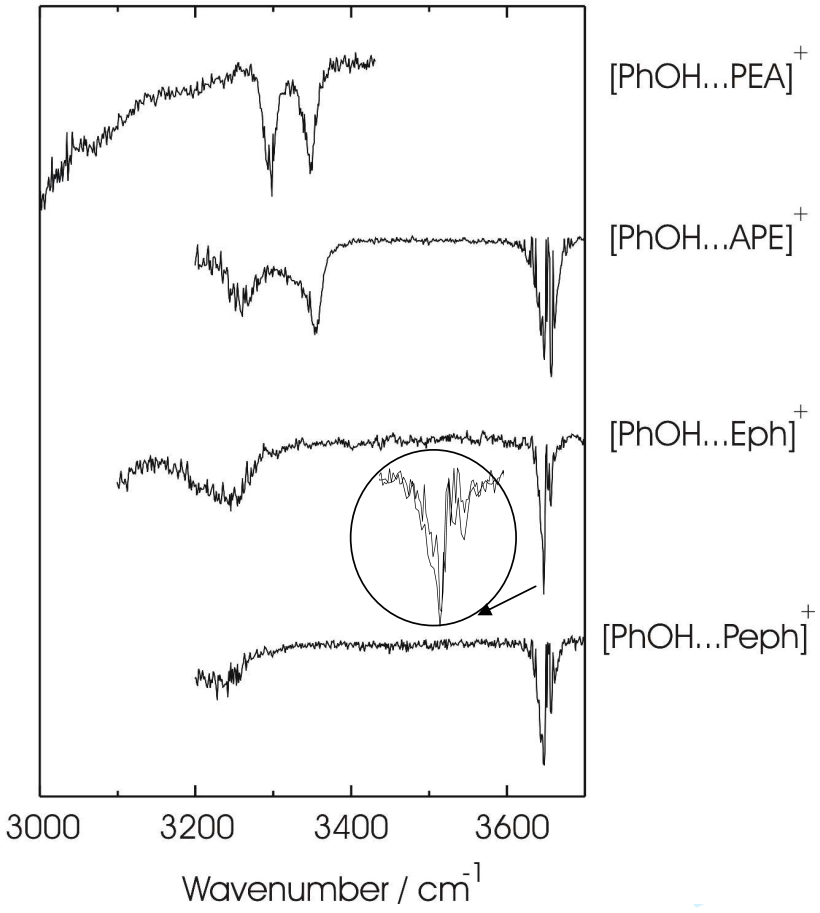

Figure 2.

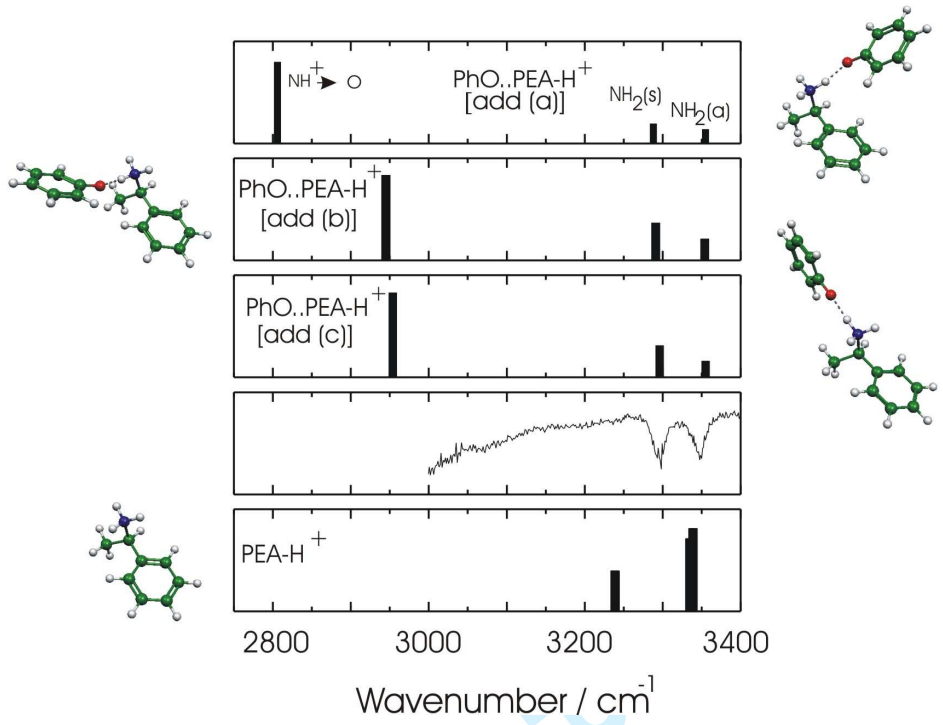

Figure 3.

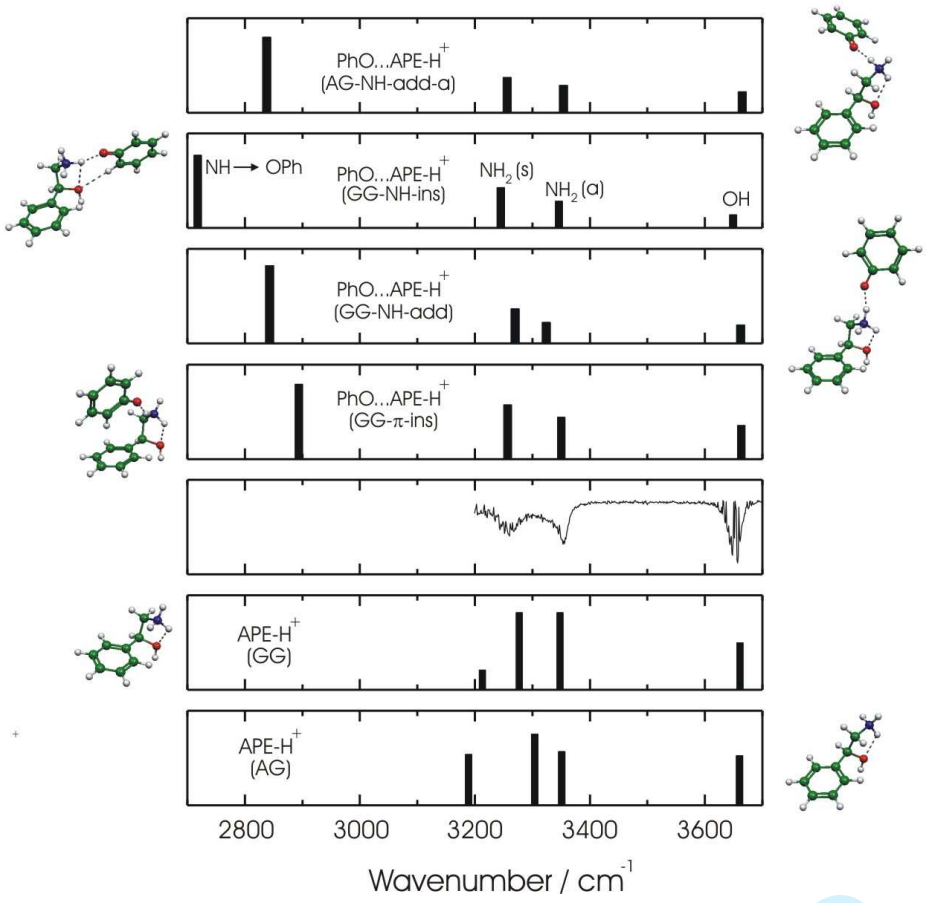

Figure 4.

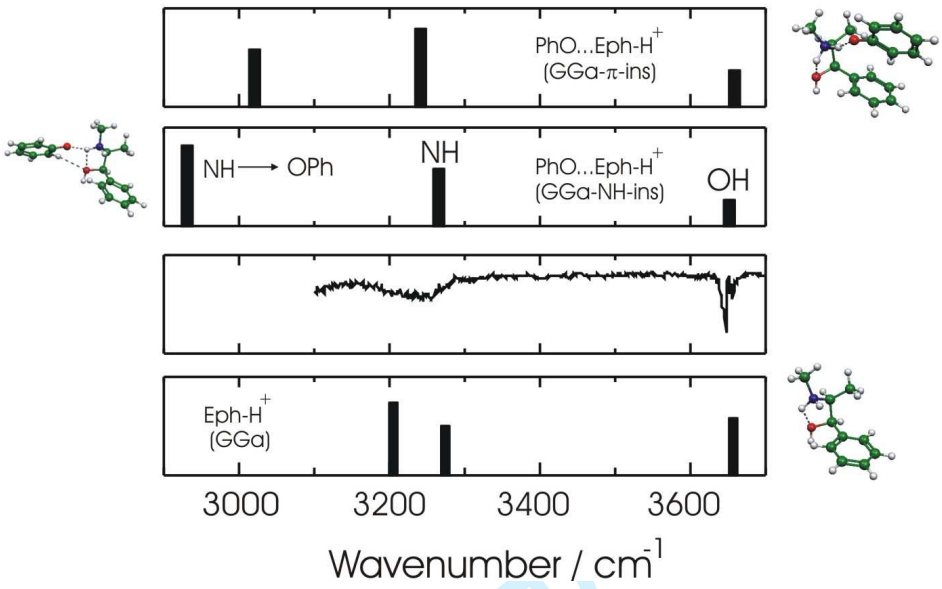

Figure 5.

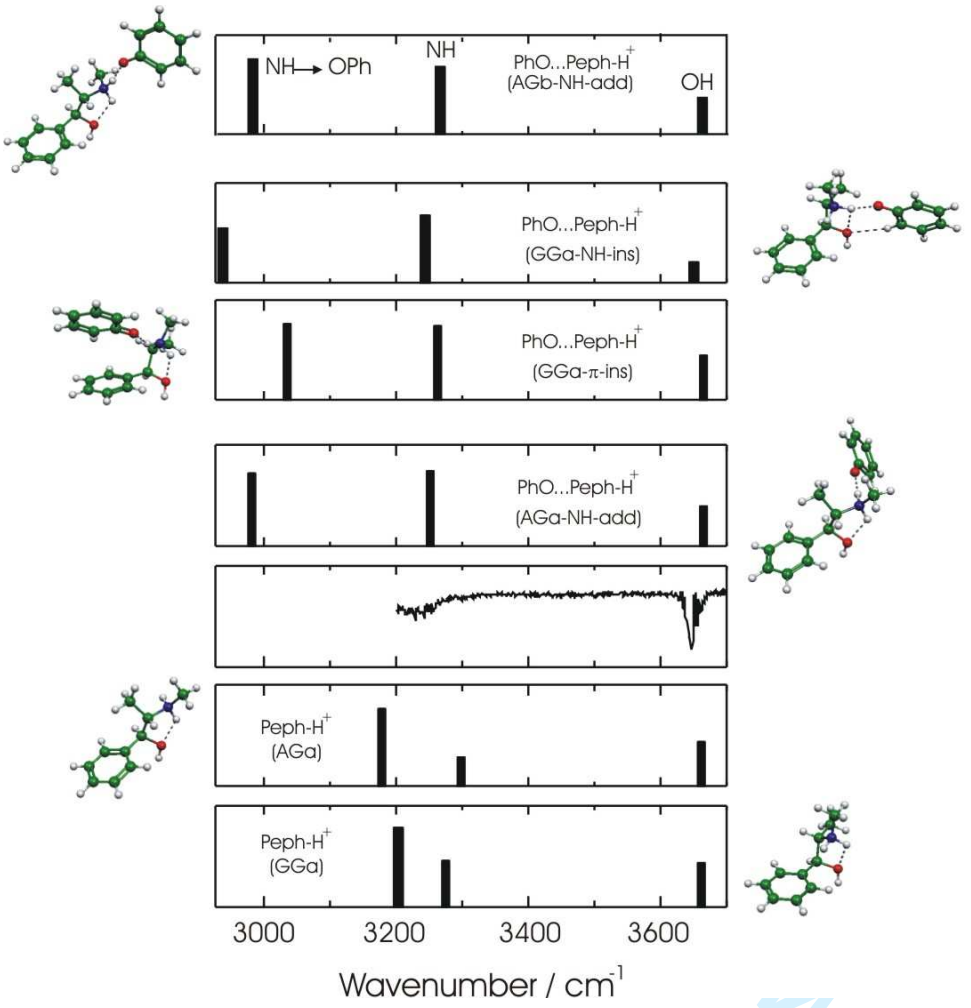

Figure 6.

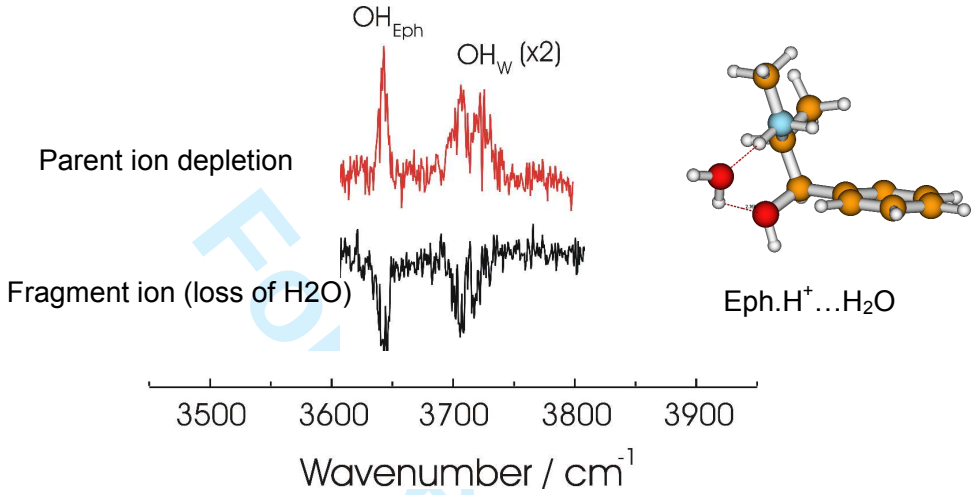

Figure 7.